Transactions of the Institute of Measurement and Control 33, 8 (2011) pp. 985–1003

Integral sliding mode control of a quadrotor with fractional order reaching dynamics

Mehmet Önder Efe

Department of Electrical and Electronics Engineering, TOBB Economics and Technology University, Ankara, Turkey

We consider integral sliding mode control with a fractional order reaching law in this paper. The reaching law approach is followed and stability of the sliding manifold is shown graphically. We choose a quadrotor-type unmanned aerial vehicle (UAV) to validate the design. The attitude dynamics of the vehicle is controlled by the proposed scheme and it is seen that the proposed form of the control system gives much better results compared with its integer order counterpart. The contribution of the study is to report a highly robust control scheme utilizing the fractional order differintegration operators.

Key words: fractional order control; quadrotor; sliding mode control.

1. Introduction

A letter from L'Hôpital to Leibniz in 1695 was asking the meaning of a derivative of order $\frac{1}{2}$. It was not until much later, only the during the last few decades, that the fractional order operators have made it possible to use automatic control systems. Considering the operator $\mathbf{D} := \mathrm{d}/\mathrm{d}t$, one could define the operators $\mathbf{D}^{\alpha}$ with a non-integer $\alpha \in \Re$. Further, for $\alpha > 0$, one obtains differentiators while $\alpha < 0$ yields integrators. In the literature, these operators are called differintegration operators

Address for correspondence: Mehmet Önder Efe, Department of Electrical and Electronics Engineering, TOBB Economics and Technology University, Sögütözü Cad. No 43, TR-06560, Sögütözü, Ankara, Turkey.
E-mail: onderefe@etu.edu.tr
Figures 1–10 appear in colour online: http://tim.sagepub.com

 10.1177/0142331210377227

and two widely used definitions are by Riemann–Liouville in (1) and by Caputo in (2) (Das, 2008; Oldham and Spanier, 1974; Ortigueira, 2000; Podlubny, 1998):

$$\mathbf{D}^{\alpha}\phi = \phi^{(\alpha)} := \frac{1}{\Gamma(n-\alpha)}\left(\frac{\mathrm{d}}{\mathrm{d}t}\right)^{n}\int_{0}^{t}\frac{\phi(\xi)}{(t-\xi)^{\alpha+1-n}}\,\mathrm{d}\xi \tag{1}$$

$$\mathbf{D}^{\alpha}\phi = \phi^{(\alpha)} := \frac{1}{\Gamma(n-\alpha)}\int_{0}^{t}\frac{\phi^{(n)}(\xi)}{(t-\xi)^{\alpha+1-n}}\,\mathrm{d}\xi \tag{2}$$

where $n-1 \leq \alpha < n$ and n is an integer. Defining $\mathcal{L}$ as the Laplace transform and s as the Laplace variable, it is possible to write $\mathcal{L}(\mathbf{D}^{\beta}) = s^{\beta}$ and such an approach makes it possible to write transfer functions in fractional orders, define the state space systems in fractional order and determine their solutions under various types of operating conditions (Das, 2008; Matignon and d'Andera-Novel, 1997; Ortigueira, 2000; Vinagre *et al*., 2002). Clearly in a significant volume of research outcomes reported so far, the linearity is an underlying assumption in the design and analysis of fractional order control systems. This paper focuses on adapting the sliding mode control technique for fractional order operators. The fundamental question answered here is as follows: is $\sigma = 0$ an attractor if a reaching law given by $\sigma^{(1+\beta)} = -\zeta\mathrm{sgn}(\sigma)$ with $\zeta > 0$ is chosen? If yes, once the error vector falls within the subspace characterized by $\sigma = 0$, the sliding manifold, it will behave according to the manifold equation, whose sole attractor is the origin.

Integral sliding mode control technique is a variant of the classical sliding mode control technique exploiting the integral of the error as the primary variable (Slotine and Li, 1991). In the past, integral sliding mode control has been used several times. Applications to stochastic systems displaying delays is considered by Niua *et al*. (2005), magnetically suspended balance beam systems by Lee *et al*. (2001), discrete time systems by Abidi *et al*. (2007), use of linear matrix inequalities in sliding surface design with integral sliding mode control is considered by Choi (2007) and pulse modulated converters operating in discrete time are elaborated on by Venkataramanan and Divan (1990). Application to the field of mobile robot control is considered by Defoort *et al*. (2006) and control of induction motors is reported by Rios-Gastelum *et al*. (2003). Clearly, the range of applications of integral sliding mode control is as wide as its conventional counterparts that have a number of applications in quadrotor control. The problem of quadrotor control is a good test bed to demonstrate the merits and effectiveness of novel control schemes, see Bouabdallah *et al*. (2004), Bouabdallah and Siegwart (2005), Castillo *et al*. (2005), Tayebi and McGilvray (2006), Xu and Özgüner (2008) and the references therein.

This paper is organized as follows. In Section 2 we present integral sliding mode control with a fractional order reaching law approach and related issues. In Section 3 we present the dynamic model of the quadrotor and describe the control problem.

In Section 4 we describe the problem of power loss and its alleviation using neural networks that complete the dynamic model. The Cartesian controller and the results obtained through a set of simulations are presented in Section 5 and concluding remarks are given at the end of the paper.

2. Integral sliding mode control with a fractional order reaching law

Sliding mode control has been a very popular control scheme experimented with on various types of real-time dynamical systems admitting switching-type control signals. Robotics is one prime area of application where tracking precision along various types of trajectories is often sought. The philosophy of the scheme is based upon the creation of an attractor in the phase space, typically spanned by the error and its time derivative, and once the point travelling within the phase space is captured by the attractor, the behaviour thereafter is governed by the subspace, called the sliding manifold. The latter dynamic behaviour is called the sliding mode due to the guidance of the error vector toward the origin of the phase space in a manner that slides along the sliding manifold. The phase lasting until the first contact with the sliding manifold is called the reaching phase and the law rendering the sliding subspace an attractor is called the reaching law (Gao and Hung, 1993; Young *et al.*, 1999). No matter what the differentiation order, the general description of SMC is as described above yet demonstrating the attractiveness of the sliding subspace is a problem remedied in this paper.

The standard design steps of the sliding mode control scheme is as follows. Consider the nonlinear dynamic system given as $\ddot{\mathbf{x}} = f(\mathbf{x}, \dot{\mathbf{x}}) + \Delta_f + \big(g(\mathbf{x}, \dot{\mathbf{x}}) + \Delta_g\big)u$. In this representation, $\mathbf{x}$ and $\dot{\mathbf{x}}$ are the state variables, $f(\mathbf{x}, \dot{\mathbf{x}})$ and $g(\mathbf{x}, \dot{\mathbf{x}})$ are smooth functions of the state variables referring to the known nominal part, Δ_f and Δ_g denote the unknown but bounded functions of the state variables and time. In addition, u is the input and $g(\mathbf{x}, \dot{\mathbf{x}}) \neq 0$. Consider the reference trajectory for position $\mathbf{x}_r$, which is differentiable, and for velocity $\dot{\mathbf{x}}_r$. Define the positional tracking error $e_{\mathbf{x}} := \mathbf{x} - \mathbf{x}_r$ and its derivative $\dot{e}_{\mathbf{x}} := \dot{\mathbf{x}} - \dot{\mathbf{x}}_r$. Based on these variables, set the switching function as $\sigma := \dot{e}_{\mathbf{x}} + \lambda e_{\mathbf{x}}$, $\lambda > 0$ is the parameter determining the slope of the sliding line. If a control law forces $\sigma = 0$ for $t \geq t_0$, then one obtains $e_{\mathbf{x}}(t) = e_{\mathbf{x}}(t_0)\ \exp(-\lambda(t - t_0))$, $t \geq t_0$. With a positive valued Q, choosing the reaching law $\dot{\sigma} = -Q\,\mathrm{sgn}(\sigma)$ would force any initial error vector to $\sigma = 0$ in finite time as the time derivative of a Lyapunov function $V = \frac{1}{2}\sigma^2$ is negative definite for $\sigma \neq 0$. Calculating the derivative $\dot{\sigma}$ and equating it to $-Q\ \mathrm{sgn}(\sigma)$ then solving for the input (u) yields the control law in (3), where we utilize solely the information about the known nominal part:

$$u = \frac{1}{g(\mathbf{x}, \dot{\mathbf{x}})}\big(\ddot{\mathbf{x}}_r - Q\,\mathrm{sgn}(\sigma) - \lambda \dot{e}_{\mathbf{x}} - f(\mathbf{x}, \dot{\mathbf{x}})\big) \tag{3}$$

Substituting the control law into the system dynamics with uncertainties lets us have

$$\dot{\sigma} = -Q\,\mathrm{sgn}(\sigma) + \Delta_f + \Delta_g u \tag{4}$$

Clearly if $\sup_{\mathbf{x},\dot{\mathbf{x}},t}|\Delta_f + \Delta_g u| < Q$, then $\sigma\dot{\sigma} < 0$ is satisfied and the subspace defined by $\sigma = 0$ becomes an attracting subspace making the overall feedback control system insensitive when the error is trapped within it. It is also possible to derive an upper bound for the time of first contact with the sliding line, say t_h. In this case, $\dot{e}_{\mathbf{x}} = -\lambda e_{\mathbf{x}}$ and we have $t_h < |\,\sigma(0)\,|\,/Q$.

Integral sliding mode control in integer order modifies the switching function as $\sigma := (\mathbf{D} + \lambda)^2\tilde{e}_{\mathbf{x}}$, where $\tilde{e}_{\mathbf{x}} := \int_0^t e_{\mathbf{x}}(\xi)\,\mathrm{d}\xi$. This clearly implies the new switching function in (5) and, according to the aforementioned procedure, the control signal in (6):

$$\sigma = \dot{e}_{\mathbf{x}} + 2\lambda e_{\mathbf{x}} + \lambda^2 \int_0^t e_{\mathbf{x}}(\xi)\,\mathrm{d}\xi \tag{5}$$

$$u = \frac{1}{g(\mathbf{x},\dot{\mathbf{x}})}\left(\ddot{\mathbf{x}}_r - Q\,\mathrm{sgn}(\sigma) - 2\lambda\dot{e}_{\mathbf{x}} - \lambda^2 e_{\mathbf{x}} - f\,(\mathbf{x},\dot{\mathbf{x}})\right) \tag{6}$$

The control law above enforces the switching variable

$$\sigma := (\mathbf{D} + \lambda)^2\tilde{e}_{\mathbf{x}} \tag{7}$$

to zero thereby leading to the emergence sliding regime after a contact with the sliding surface in finite time. The modification by considering the integral of the error instead of the error itself makes the overall control scheme more robust against disturbances (Abidi *et al*., 2007; Choi, 2007; Defoort *et al*., 2006; Lee *et al*., 2001; Niua *et al*., 2005; Rios-Gastelum *et al*., 2003; Venkataramanan and Divan, 1990).

The traditional approaches summarized so far consider the integer order derivatives as the theory and practice lying behind is well founded and many successful applications were reported in the literature. We now choose the reaching law as given by (8) with $0 < \beta < 1$:

$$\sigma^{(1+\beta)} = -Q\,\mathrm{sgn}(\sigma) \tag{8}$$

In order to obtain $\dot{\sigma}$, we differentiate (8) to the order $-\beta$, which corresponds to integrating (8) to the order β. This would let us have

$$\dot{\sigma} = -Q\,\mathbf{D}^{-\beta}\mathrm{sgn}(\sigma) \tag{9}$$

On the other hand, the first derivative of (7) with respect to time yields

$$\dot{\sigma} = (\mathbf{D} + \lambda)^2 e_{\mathbf{x}} \tag{10}$$

$$= \ddot{e}_{\mathbf{x}} + 2\lambda e_{\mathbf{x}} + \lambda^2 e_{\mathbf{x}} \tag{11}$$

$$= \ddot{\mathbf{x}} - \ddot{\mathbf{x}}_r + 2\lambda e_{\mathbf{x}} + \lambda^2 e_{\mathbf{x}} \tag{12}$$

$$= f\,(\mathbf{x},\dot{\mathbf{x}}) + g(\mathbf{x},\dot{\mathbf{x}})u - \ddot{\mathbf{x}}_r + 2\lambda e_{\mathbf{x}} + \lambda^2 e_{\mathbf{x}} \tag{13}$$

Equating (13) to (11) and solving for u yields the following control law that contains the integral of the switching variable at order β:

$$u = \frac{1}{g(\mathbf{x}, \dot{\mathbf{x}})}\left(\ddot{\mathbf{x}}_r - Q\,\mathbf{D}^{-\beta}\mathrm{sgn}(\sigma) - 2\lambda\dot{e}_{\mathbf{x}} - \lambda^2 e_{\mathbf{x}} - f(\mathbf{x}, \dot{\mathbf{x}})\right) \tag{14}$$

Regarding the stability of the closed-loop control system exploiting the control law in (14), one has to figure out whether $\sigma = 0$ is an attractor, or not. In Figure 1, the time solution of the reaching dynamics is given for unity initial condition and for various β values. Clearly, $\sigma = 0$ is reached in all cases yet every trajectory has its own transient characteristics. Recall (9) with the Riemann–Liouville definition of the fractional order integration in (1). Since $0 < \beta < 1$, we have $\mathrm{sgn}(\mathbf{D}^{-\beta}\,\mathrm{sgn}(\sigma)) = \mathrm{sgn}(\sigma)$ and this leads us to deduce that a control law forcing $\sigma^{(1+\beta)}\sigma < 0$ would also force $\sigma\dot{\sigma} < 0$ initially. Therefore, the control law in (14) renders the subspace defined by $\sigma = 0$ an attractor. In Figure 2, the convergence is depicted for $\beta = 0.5$. Two initial conditions are studied and the results are plotted on the axes $\dot{\sigma}$ versus σ. It is seen that the trajectories follow a particular pattern while converging to the origin and numerically it is seen that the origin is a stable attractor.

Let $\mathcal{S} := \{t_{h_0}, t_{h_0}, \ldots, t_{h_n}\}$ be the set of time instants corresponding to switching times. Let t_{h_0} be zero and $c_k := (-1)^k(u_k + u_{k-1})$ and $u_k = 1$ for $k \geq 0$, zero otherwise.

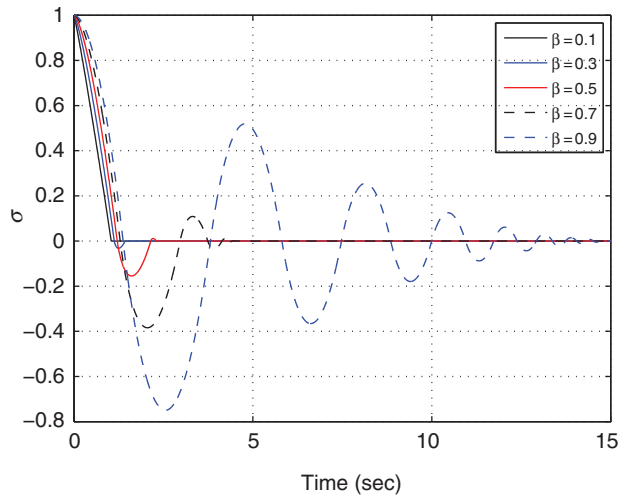

Figure 1 The solution of $\sigma^{(1+\beta)} = -\zeta\ \mathrm{sgn}(\sigma)$ for $\zeta = 1$ and for $\sigma(0) = 1$

Having these in mind, we can postulate the following solution to use in the right-hand side of (9):

$$\mathbf{D}^{-\beta}\mathrm{sgn}(\sigma) = \frac{\mathrm{sgn}(\sigma(0))}{\Gamma(\beta+1)}\sum_{k=0}^{n} c_k(t-t_{h_k})^{\beta}$$

where $t_{h_n} \le t \le t_{h\ n+1}$. Clearly when $t = t_{h_k}$ for $k \ge 1$, we have $\sigma(t_{h_k}) = 0$, which is solved explicitly as in (15):

$$\sigma(t) = \sigma(t_{h_n}) - \frac{Q\mathrm{sgn}(\sigma(0))}{\Gamma(\beta+2)}\sum_{k=0}^{n} c_k\left((t-t_{h_k})^{\beta+1} - (t_{h_n}-t_{h_k})^{\beta+1}\right), \quad n = 1,2,\ldots,\infty \tag{15}$$

Regarding the solution above, when $n=1$, ie, $0 = t_{h_0} \le t \le t_{h_1}$, we have $\sigma(t) = \sigma(0) - \frac{Q\mathrm{sgn}(\sigma(0))}{\Gamma(\beta+2)}(t-t_{h_0})^{\beta+1}$. From this, it can be shown that the first contact occurs at t_{h_1} given as follows:

$$t_{h_1} = \left(\frac{|\sigma(0)|\Gamma(\beta+2)}{Q}\right)^{\frac{1}{\beta+1}} \tag{16}$$

For $|\sigma(0)| = 1$, $\zeta = 1$ and $\beta = 0.5$, one obtains $t_{h_1} = 1.209\,\mathrm{s}$, which is the value seen in Figure 1 as well. When $n=2$, ie, $t_{h_1} \le t \le t_{h_2}$, the second hitting time is solved from the following equation:

$$(t_{h_2}-t_{h_0})^{\beta+1} - (t_{h_1}-t_{h_0})^{\beta+1} - 2(t_{h_2}-t_{h_1})^{\beta+1} = 0 \tag{17}$$

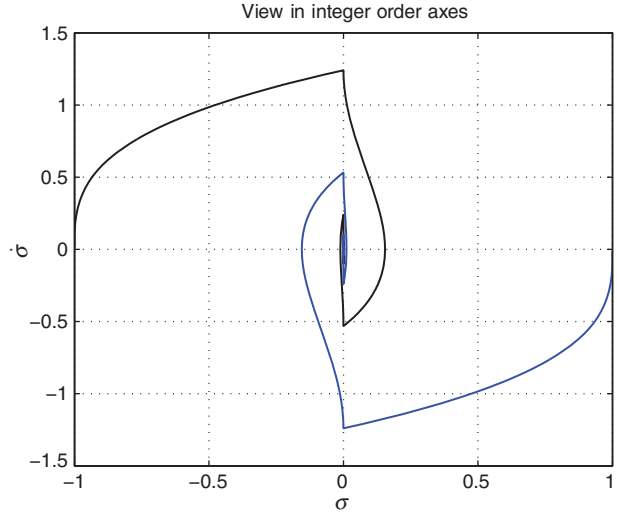

Figure 2 Integer order phase space trajectories of the solution of $\sigma^{(1+\beta)} = -\zeta\ \mathrm{sgn}(\sigma)$ for $\zeta = 1$ and for $\sigma(0) = \pm 1$

Similarly, for the computation of t_{h_3}, one needs to solve the following algebraic equation:

$$\begin{aligned}(t_{h_3}-t_{h_0})^{\beta+1}-(t_{h_2}-t_{h_0})^{\beta+1}-2(t_{h_3}-t_{h_1})^{\beta+1}\\ +2(t_{h_2}-t_{h_1})^{\beta+1}+2(t_{h_3}-t_{h_2})^{\beta+1}=0\end{aligned} \tag{18}$$

Unfortunately, as n increases, the complexity of the equation to be solved increases and it only becomes possible to show the result via numerical techniques as seen in Figure 1, where we see that $\sigma=0$ is a global attractor.

3. Quadrotor dynamics

The vehicle considered in this study is illustrated in Figure 3 and the physical parameters are listed in Table 1. The dynamical equations describing the quadrotor rotorcraft are given in (19)–(24), where the first three of these equations describe the dynamics in the Cartesian space, whereas the last three express the dynamics in the Euler angles, ie, the attitude. The state of the system is characterized by the translational and angular positions and velocities, ie, x, y, z, $\dot{x}$, $\dot{y}$, $\dot{z}$, ϕ, θ, ψ, $\dot{\phi}$, $\dot{\theta}$ and $\dot{\psi}$. The control input for the translational dynamics is denoted by U_1. The control inputs

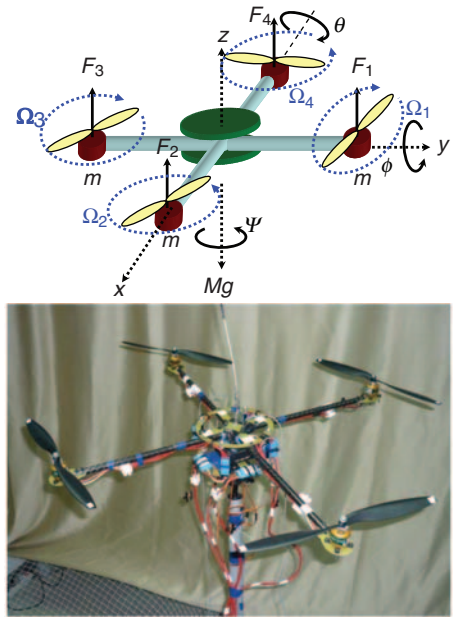

Figure 3 Top: Schematic view and variable definitions of a quadrotor type unmanned aerial vehicle (UAV). Bottom: Real implementation used to determine b and d coefficients

influencing the attitude of the vehicle are U_2 for the roll axis, U_3 for the pitch axis and U_4 for the yaw axis:

$$\ddot{x} = (\cos\phi \sin\theta \cos\psi + \sin\phi \sin\psi)\frac{1}{M}U_1 \tag{19}$$

$$\ddot{y} = (\cos\phi \sin\theta \sin\psi - \sin\phi \cos\psi)\frac{1}{M}U_1 \tag{20}$$

$$\ddot{z} = -g + \cos\phi \cos\theta \frac{1}{M}U_1 \tag{21}$$

$$\ddot{\phi} = \dot{\theta}\dot{\psi}\left(\frac{I_{yy} - I_{zz}}{I_{xx}}\right) + \frac{j_r}{I_{xx}}\dot{\theta}\Upsilon + \frac{L}{I_{xx}}U_2 \tag{22}$$

$$\ddot{\theta} = \dot{\phi}\dot{\psi}\left(\frac{I_{zz} - I_{xx}}{I_{yy}}\right) - \frac{j_r}{I_{yy}}\dot{\phi}\Upsilon + \frac{L}{I_{yy}}U_3 \tag{23}$$

$$\ddot{\psi} = \dot{\theta}\dot{\phi}\left(\frac{I_{xx} - I_{yy}}{I_{zz}}\right) + \frac{1}{I_{zz}}U_4 \tag{24}$$

Denoting the lifting force created by the ith motor–propeller pair by F_i and the corresponding angular velocity by Ω_i, in (25)–(29), the definitions of the control inputs and the term Υ seen in the unmanned aerial vehicle (UAV) dynamics are given by:

$$U_1 = b\Omega_1^2 + b\Omega_2^2 + b\Omega_3^2 + b\Omega_4^2 = \sum_{i=1}^{4} F_i \tag{25}$$

$$U_2 = b\Omega_4^2 - b\Omega_2^2 = F_4 - F_2 \tag{26}$$

$$U_3 = b\Omega_3^2 - b\Omega_1^2 = F_3 - F_1 \tag{27}$$

$$U_4 = d\,(\Omega_1^2 - \Omega_2^2 + \Omega_3^2 - \Omega_4^2) \tag{28}$$

$$\Upsilon = \Omega_1 - \Omega_2 + \Omega_3 - \Omega_4 \tag{29}$$

Table 1 Physical parameters of the quadrotor unmanned aerial vehicle

L	Half distance between two motors	0.3 m
M	Mass of the vehicle	0.8 kg
g	Gravitational acceleration constant	9.81 m/s^2
I_{xx}	Moment of inertia around x-axis	15.67×10^{-3}
I_{yy}	Moment of inertia around y-axis	15.67×10^{-3}
I_{zz}	Moment of inertia around z-axis	28.346×10^{-3}
b	Thrust coefficient	192.3208×10^{-7} Ns^2
d	Drag coefficient	4.003×10^{-7} Nms^2
j_r	Propeller inertia coefficient	6.01×10^{-5}

The control problem here is to drive the UAV toward a predefined trajectory in the 3D space by generating an appropriate sequence of Euler angles, which also needs to be controlled. The latter is called attitude control and the command signals to which are produced by the Cartesian controller.

4. Power loss compensation using neural networks

The dynamical model of a UAV such as that considered in this paper is obtained using the laws of physics. Principally, a control signal to be applied to the motors must be converted to pulse width modulation (pwm) signals then electronic speed controllers properly drive the brushless motors, and a thrust value is obtained from each motor–propeller pair. The numerical value of the thrust is dependent upon the type of the propeller and the angular speed of the rotor in radians as $F_i = b\Omega_i^2$ where F_i is the thrust at the ith motor, b is a constant-valued thrust coefficient and Ω_i is the angular speed in radians per second. If the control inputs (thrusts) needed to observe a desired motion were immediately available, then it would be easier to proceed to the closed-loop control system design without worrying about the effects of the actuation periphery, which introduces some constraints shaping the transient and steady-state behavior of the propulsion. Indeed, the real-time picture is complicated as the control signals are torques produced by motor–propeller pairs introducing certain transient characteristics, further, the vehicle is powered electrically, where the battery voltage is reducing gradually. Such a change in the battery voltage causes different lift forces at different battery voltage levels although the applied pwm level is constant as shown in Figure 4. The same 42-second pwm profile in Figure 4 is applied 40 times and as the

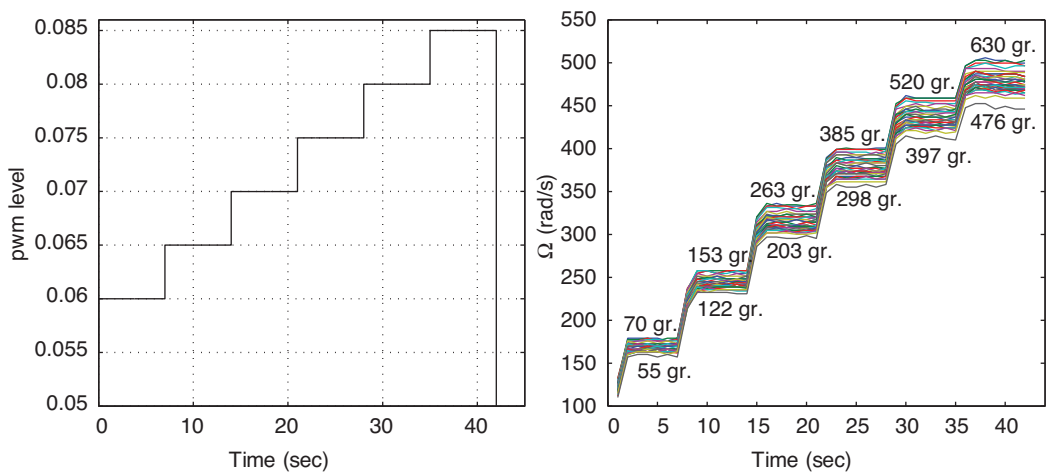

Figure 4 Left: Applied pwm profile. Right: Decrease in the angular speed as the battery voltage decreases

battery voltage reduces the angular speed at a constant pwm level decreases thereby causing a decrease in the generated thrust. Furthermore, the relation with different pwm levels is not linear, ie, the same amount of change in the input causes different amounts of change at different levels, and this shows that the process to be modeled is nonlinear.

According to Figure 4, comparing the fully charged condition of the battery and the condition at the last experiment displays 15 g of difference for the lowest level, 154 g at the highest level, which is obviously an uncertainty that has to be incorporated into the dynamic model and the feedback controller appropriately. The use of neural networks is a practical alternative to resolve the problem induced by battery conditions. Using $V_b(t)$ to denote the battery voltage, a neural network model performing the map $y_{\text{pwm}} = \text{NN}(\Omega_c, V_b)$ is the module installed to the output of a controller generating the necessary angular speeds. Here Ω_c is the angular speed prescribed by the controller. Another neural network that implements $y_\Omega = \text{NN}(V_b,$ pwm, $H_2(\text{pwm}))$ is the module installed to the inputs of the dynamic model of the UAV. The box with $H_2(\cdot)$ is a low pass filter incorporating the effect of transient in the thrust value. The dynamic model contains F_i that are computed using Ω_i.

The reason why we would like to step down from thrusts to the pwm level and step up from pwm level to forces is the fact that brushless DC motors are driven at the pwm level and one has to separate the dynamic model of the UAV and the controller by drawing a line exactly at the point of signal exchange occurring at the pwm level. The use of neural networks facilitates this in the presence of voltage loss in the batteries.

In Figure 5, the diagram describing the role of aforementioned offline trained neural models are shown. In Figure 6, the results obtained with real-time data are shown. A chirp-like pwm profile was generated and some noise was added to obtain a pwm signal to be applied. When this signal is applied as an input to any motor, the variation in the battery voltage is measured and filtered to guide the neural models as shown in the top right subplot. After that, the corresponding angular speed is

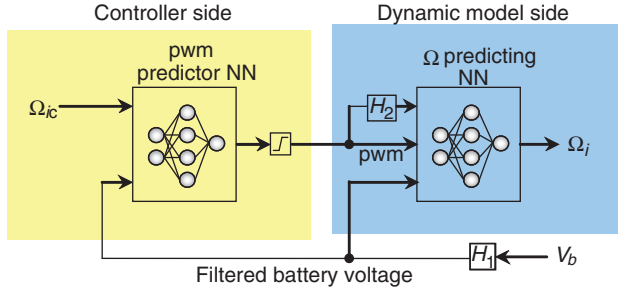

Figure 5 Installing the neural network components for hand-shaking at pwm level, whose applicable range is [0.050, 0.085]

computed experimentally. In the middle left subplot, the reconstructed pwm signal and the applied signal are shown together. In the middle right subplot, the performance for the angular speed (Ω) predicting neural model is depicted. Both subplots of the middle row of the figure suggest a useful reconstruction of the signal obtained from the neural networks that were trained by using Levenberg–Marquardt algorithm. In both models, the neural networks have a single hidden layer with hyperbolic tangent-type neuronal nonlinearity and linear output neurons. The pwm

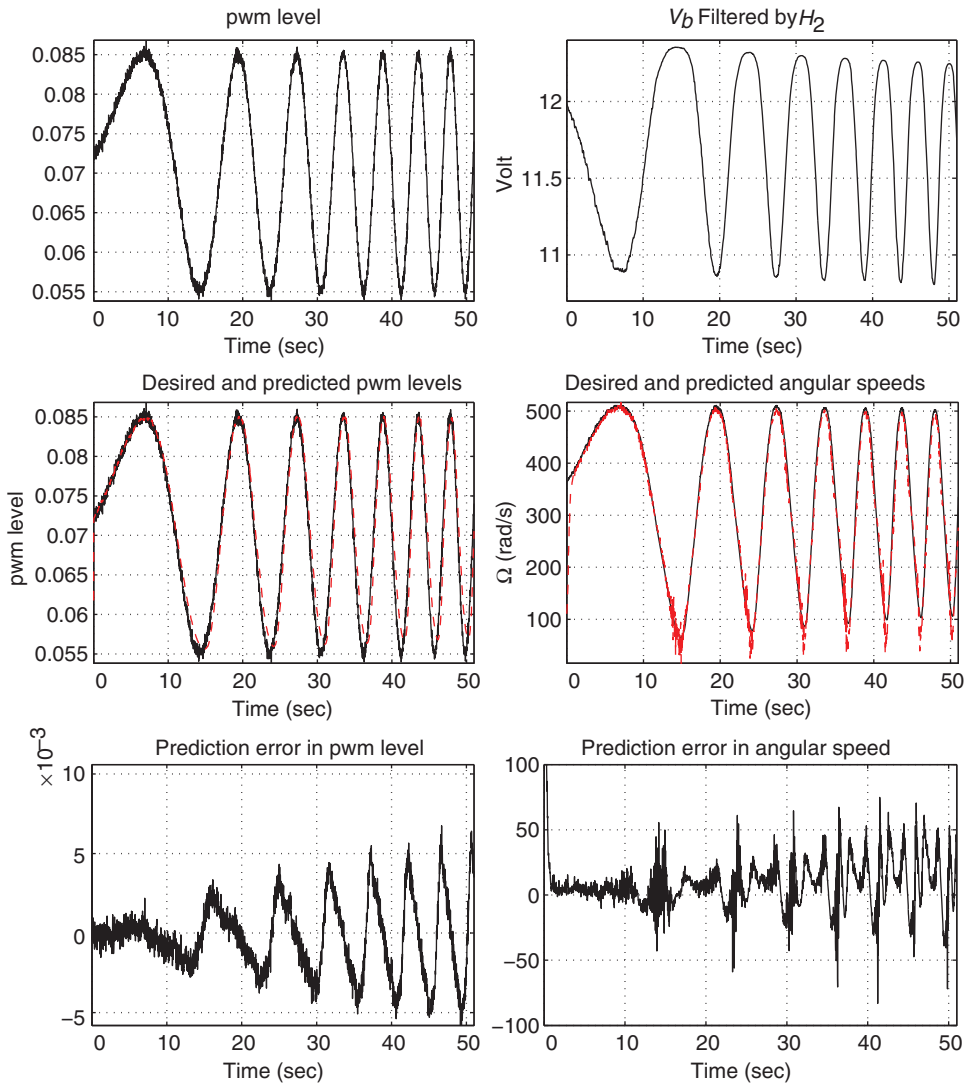

Figure 6 Performance of the two neural network models

predicting model has 12 hidden neurons with a final mean squared error (MSE) value of 90.8285×10^{-4}, which is for 88 400 pairs of training data. Angular speed predicting neural model has 10 hidden neurons with a final MSE value 3.9208×10^{-4} for 62 050 pairs of training data collected utilizing a DS1104 data acquisition system.

Bottom subplots of Figure 6 illustrate the difference between the desired and predicted values. As the local frequency of the target output increases, the neural models start performing poorer yet the performance is good when the signals change slowly. This is an expected result that is in good compliance with the typical real-time signals obtained from a quadrotor-type UAV discussed in the third section.

5. Simulation results

Denote the reference Cartesian positions and velocities by r_x, r_y, r_z and $\dot{r}_x$, $\dot{r}_y$, $\dot{r}_z$. We define $P_z := -4\dot{z} - 4(z - r_z)$ and choose the altitude controller as given in (30):

$$U_1 = M\frac{P_z + g}{\cos\theta\cos\phi} \tag{30}$$

Substituting (30) into (19) and (20), and adopting the small angle approximation would let us obtain the following dynamics:

$$\ddot{x} \approx (P_z + g)\tan\theta \tag{31}$$

$$\ddot{y} \approx -(P_z + g)\tan\phi \tag{32}$$

In the above dynamics, $\tan\phi$ and $\tan\theta$ can be regarded as the control inputs for observing the desired motion in Cartesian space. To achieve this, following choices are made

$$\phi_r = -\arctan\left(\frac{P_y}{P_z + g}\right) \tag{33}$$

$$\theta_r = \arctan\left(\frac{P_x}{P_z + g}\right) \tag{34}$$

where $P_x = -\dot{x} - (x - r_x)$ and $P_y = -\dot{y} - (y - r_y)$. Now we utilize the fractional order integral sliding mode controller explained in the Section 2 to track these Euler angles to obtain the desired motion. The simulations have been carried out with the settings given in Table 2.

The other practical considerations implemented are listed below.

- A common problem of the sliding mode control systems is the presence of a chattering phenomenon, that is a natural consequence of the scheme checking the sign of a quantity that is close to zero. The robustness is dependent upon the value of ζ, and

Table 2 Simulation settings

β	Fractional order	0.5
Δt	Simulation stepsize	1 ms
T	Final time	130 s
λ	Slope parameter	1
ζ	Reaching law parameter	10
$(\phi(0), \theta(0), \psi(0))$	Initial attitude of the vehicle	$\left(\frac{\pi}{7}, -\frac{\pi}{6}, -\frac{\pi}{5}\right)$
$(x(0), y(0), z(0))$	Initial position of the vehicle	$(-2, 3, 0)$

if a larger ζ is chosen, theoretically the system becomes more capable of alleviating uncertainties of larger magnitudes yet this provokes the switching nature of the control signal and the performance degrades significantly. Further, chattering is magnified and the control system becomes practically infeasible. A remedy is to introduce a sign function smoothing, yet this introduces a boundary layer and reduces from the performance. In the current study, due to the design presented, a (relatively) large value for ζ is chosen and no smoothing is performed on the sign function.

- The UAV developed in the laboratory is powered by lithium–polymer type batteries and it is shown that the outrunner brushless DC motors claim very high currents causing a significant reduction in the battery voltage. This causes an uncertainty to be alleviated by the controller as the same input signal causes different lift forces as the battery voltage drops in time. Owing to space limitations, the details are not presented here but the change in the battery voltage is simulated as an exponentially converging value starting from 11.1 V to 9.9 V in 130 seconds of flight. For details refer to Köroglu *et al*. (2009).
- Aside from the initial conditions given in Table 2, the remaining set of initial conditions are chosen to be zero, ie, the vehicle is motionless initially. Since the goal is to demonstrate the performance of the proposed fractional order sliding mode control scheme, it is adequate to assume non-zero positional initial values for the Euler angles and x and y coordinates.
- In order to demonstrate the robustness against disturbances, the angular speeds of the vehicle have been perturbed additively to simulate the effect of weather conditions, such as wind. The perturbations modify the angular speeds to $\Omega_i + K \sin(2\pi t/T_i)$, where $T_1 = 10$ s, $T_2 = 12$ s, $T_3 = 14$ s, $T_4 = 16$ s and $K = 8$.
- The observations are noisy, the state vector composed of the positions and velocities are corrupted by noise sequences of power 1×10^{-4}, which is large enough to test the performance of the proposed control scheme.
- Since we need the angular speeds without installing any rpm sensors, the term Υ is computed by utilizing the prescribed control signals

$$\Upsilon(t) \approx \Omega_{1c}(t-\tau) - \Omega_{2c}(t-\tau) + \Omega_{3c}(t-\tau) - \Omega_{4c}(t-\tau) \tag{35}$$

where τ is a small delay removing the algebraic loop problems. Although it was possible to choose a smaller value, in the simulations $\tau = 0.1$ s has been selected to see

how robust the overall control system is.

- Finally, the implementation of fractional order operators need to be discussed. During the simulations, the numerical implementation of the control law in (6) is achieved through the use of well-known Crone approximation, which prescribes a series of poles and zeros to build a transfer function $k\prod_{i=1}^{N}(1+s/z_i)/(1+s/p_i)$ approximating the desired operator spectrally (Valério, 2005). We choose $N=9$ and a frequency range covering 0.001 to 1000 rad/s to realize these operators. Regarding the choice $\beta=0.5$, following remarks are useful. For $\beta=0$, classical design is obtained, and in this case, the closed-loop system is not more robust than the case with $0<\beta<1$. At the other extreme, when $\beta=1$, the attractiveness of $\sigma=0$ is lost. Such a behavioral spectrum indicates that there is a good value of β such that $\sigma=0$ is an attractor and the closed-loop system displays the desired robustness properties. Based on these observations, this paper considers $\beta=0.5$.

  As β approaches zero, the robustness is lost smoothly and many contacts take place before the sliding regime starts; on the other hand, as β approaches zero, the errors signals are deteriorated and the control system becomes extremely vulnerable to noise. This naturally suggests choosing $\beta=0.5$, which is equally distant to the mentioned undesired regimes.

Under the aforementioned conditions, the results shown in Figure 7 are obtained. According to the trajectories depicted in the top left subplot of the figure, the vehicle is seen to follow the desired path closely. The other three

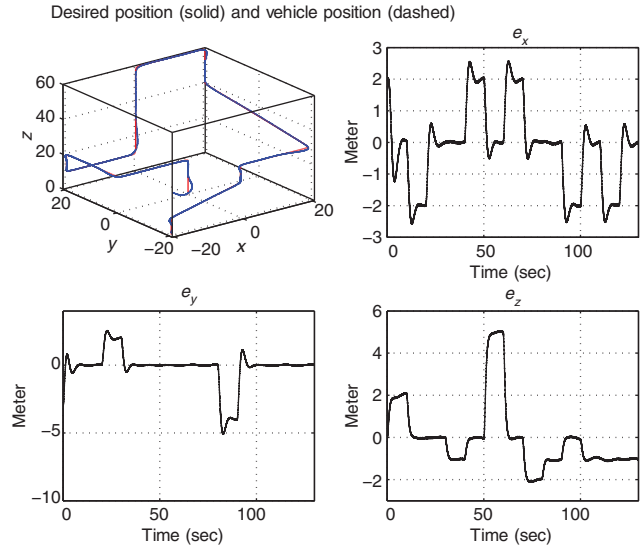

Figure 7 Results for the Cartesian space variables

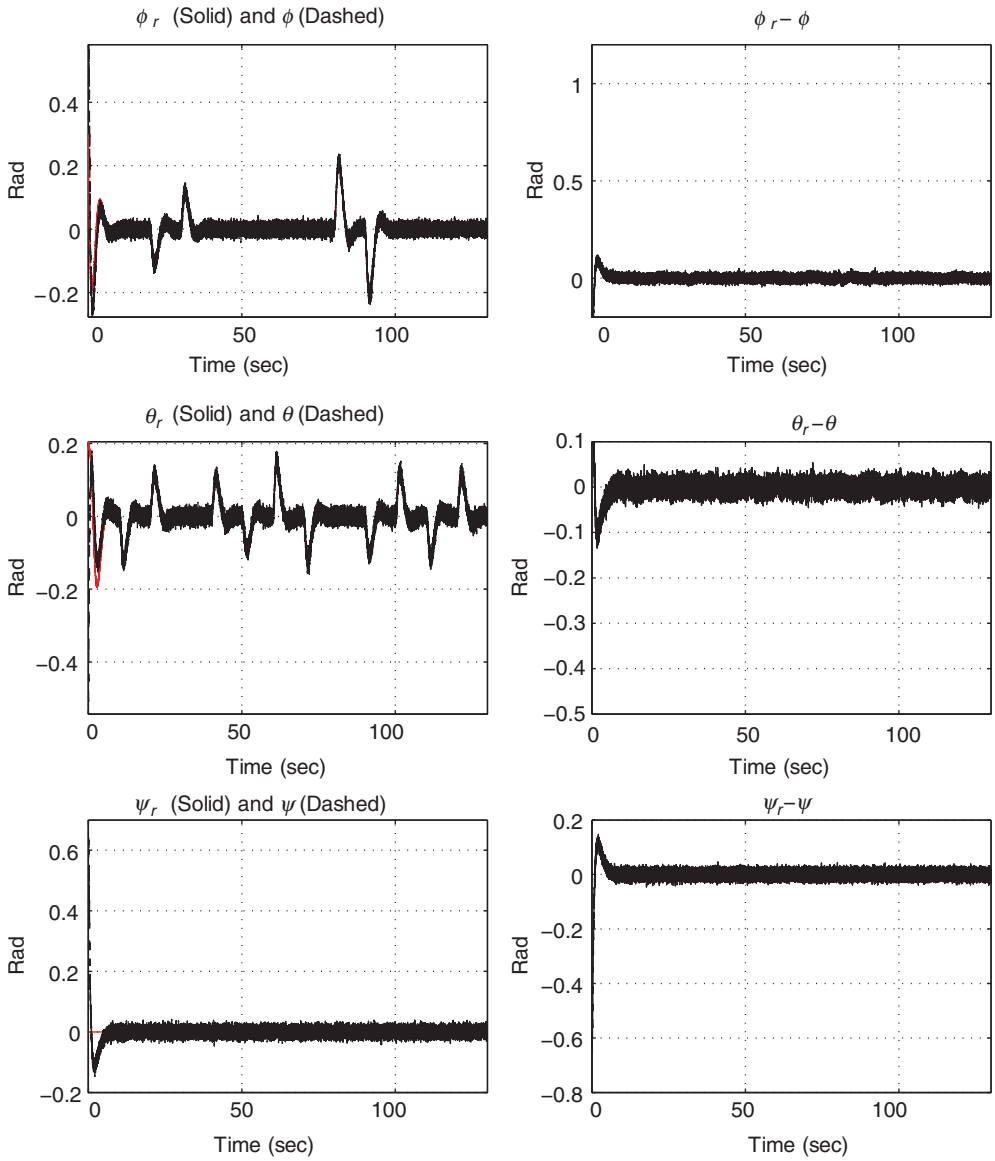

Figure 8 Results for the Euler angles (attitude)

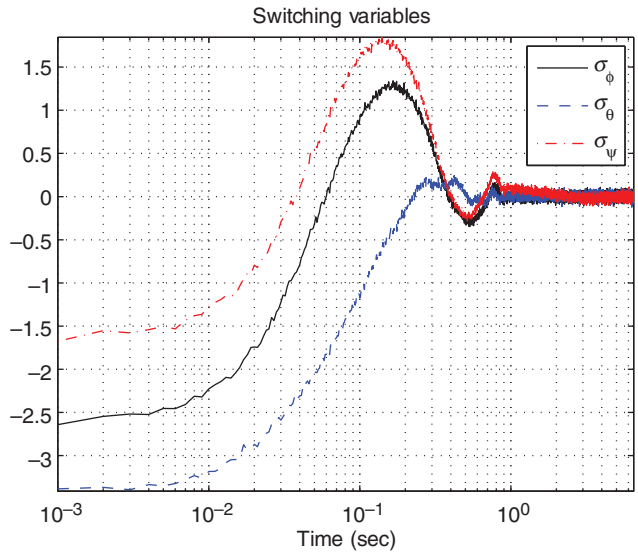

Figure 9 Time evolution of the switching variables

subplots illustrate the discrepancies observed in the Cartesian components of the dynamics. Considering the followed trajectory, the errors are seen to be tolerable yet it is possible to enhance these error trends by changing the Cartesian space controller to another one. In this work, we only implement the fractional order integral sliding mode control scheme for the attitude dynamics whose results are shown in Figure 8. The subplots on the left column depict the tracking of the prescribed Euler angles, and those on the right illustrate the tracking errors, which converge to zero after a transient phase characterized by the proposed reaching dynamics. The evolution of the switching variables (σ) for each subdynamics is shown in Figure 9, where it is seen that the switching variables converge to zero during the reaching phase and sliding mode starts after the reaching phase ends.

A comparison of the control law in (6) with the classical integral sliding mode control scheme stipulates the results shown in Figure 10. Few parameter combinations have been studied and it is seen that either the performance is poor or the closed-loop system becomes unstable. For the smaller values of wind disturbance magnitude K, the controller is able to force the UAV to track its desired trajectory, yet when $K = 8$, the controller is unable to maintain a safe flight. This simple comparison shows that the proposed scheme, despite its slightly costly nature, is a good alternative in applications requiring robustness such as that considered in this paper.

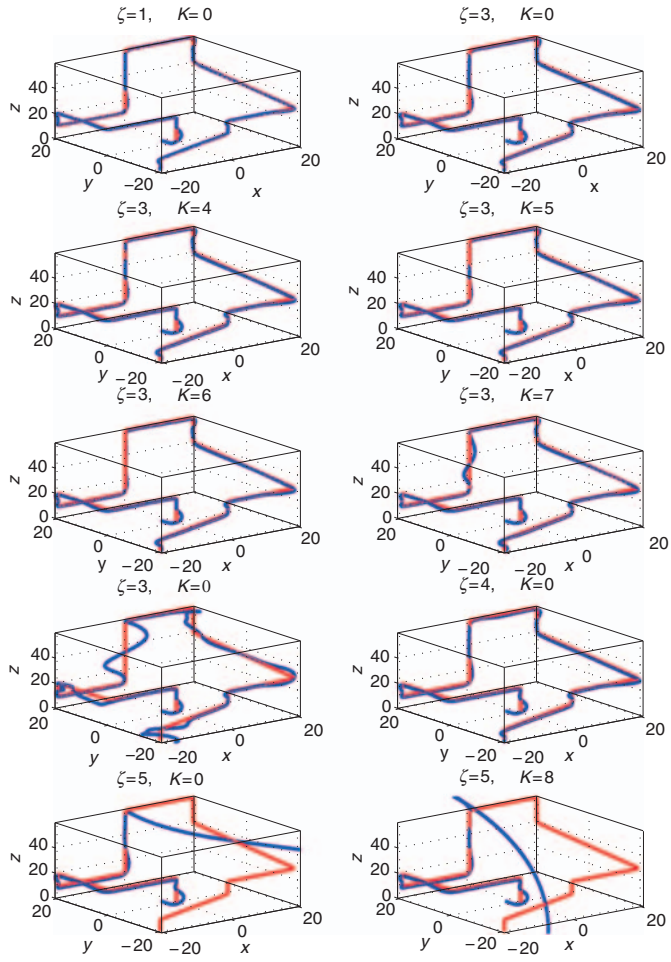

Figure 10 Results generated by the classical integral sliding mode controller with different parameter selections

6. Concluding remarks

Integral sliding mode control has been reformulated for a fractional order reaching law approach. The benefits of the classical sliding mode control are observed, further, the control system has been shown to be robust against disturbances acting on the state variables and the controller output. A quadrotor-type UAV was chosen as the test bed and it is seen that the proposed control scheme successfully drives the system toward the desired regime under the presence of loss in the battery voltage.

Compared with its integer order alternative, the proposed form of the control law enhances the trajectory tracking performance of the UAV, the control of which require robustness against disturbances and uncertainties.

Funding

This work was supported by TÜBİTAK, under contract number 107E137.

Acknowledgements

The author gratefully acknowledges the facilities of the Unmanned Aerial Vehicles Laboratory of TOBB ETÜ and fruitful discussions with Mert Önkol, Aydın Eresen, Nevrez İmamoglu and M. Taha Köroglu.

References

Abidi, K., **Xu, J.-X.** and **Yu, X.** 2007: On the discrete-time integral sliding-mode control. *IEEE Transactions on Automatic Control* 52(4): 709–15.

Bouabdallah, S., **Murrieri, P.** and **Siegwart, R.** 2004: Design and control of an indoor micro quadrotor. *Proceedings 2004 IEEE International Conference on Robotics and Automation*, Vol. 26. New Orleans, LA, 4393–8, April–1 May.

Bouabdallah, S. and **Siegwart, S.** 2005: Backstepping and sliding-mode techniques applied to an indoor micro quadrotor. *IEEE International Conference on Robotics and Automation*, Barcelona, Spain, 2247–52.

Castillo, P., **Lozano, R.** and **Dzul, A.** 2005: Stabilization of a mini rotorcraft with four rotors. *IEEE Control Systems Magazine* 45–55.

Choi, H.H. 2007: LMI-based sliding surface design for integral sliding mode control of mismatched uncertain systems. *IEEE Transactions on Automatic Control* 52(4): 736–42.

Das, S. 2008: *Functional Fractional Calculus for System Identification and Controls*. 1st edition. Springer.

Defoort, M., **Floquet, T.**, **Kokosy, A.** and **Perruquetti, W.** 2006: Integral sliding mode control for trajectory tracking of a unicycle type mobile robot. *Integrated Computer-Aided Engineering* 13(3): 277–288.

Gao, W. and **Hung, J.C.** 1993: Variable structure control of nonlinear systems: a new approach. *IEEE Transactions on Industrial Electronics* 40(1): 45–55.

Köroglu, M.T., **Önkol, M.** and **Efe, M.Ö.** 2009: Experimental modelling of propulsion transients of a brushless DC motor and propeller pair under limited power conditions: a neural network based approach. *The 2nd IFAC International Conference on Intelligent Control Systems and Signal Processing (ICONS'09)*İstanbul, Turkey, 21–23, September.

Lee, J.-H., **Allaire, P.E.**, **Tao, G.** and **Zhang, X.** 2001: Integral sliding-mode control of a magnetically suspended balancebeam: analysis, simulation, and experiment. *IEEE/ASME Transactions on Mechatronics* 6(3): 338–346.

Matignon, D. and **d'Andera-Novel, B.** 1997: Observer Based Controllers for Fractional Differential Systems. *International Conference on Decision and Control*, San Diego, CA, 4967–72.

Niua, Y., **Hob, D.W.C.** and **Lamc, J.** 2005: Robust integral sliding mode control for uncertain stochastic systems with time-varying delay. *Automatica* 41(5): 873–80.

Oldham, K.B. and **Spanier, J.** 1974: *The Fractional Calculus*. Academic Press.

Ortigueira, M.D. 2000: Introduction to fractional linear systems. Part 1: continuous

time case. *IEE Proceedings—Vision, Image, and Signal Processing* 147(1): 62–70.

Podlubny, I. 1998: *Fractional Differential Equations*. 1st edition. Elsevier Science & Technology Books.

Rios-Gastelum, O.G., **Castillo-Toledo, B.** and **Loukianov, A.G.** 2003: Nonlinear block integral sliding mode control: application to induction motor control. *Proceedings of the 42nd IEEE Conference on Decision and Control*, Maui, HI, 3124–3129.

Slotine, J.J.E. and **Li, W.** 1991: *Applied Nonlinear Control*. Prentice-Hall.

Tayebi, A. and **McGilvray, S.** 2006: Attitude stabilization of a VTOL quadrotor aircraft. *IEEE Transactions on Control Systems Technology* 14(3): 562–71.

Valério, D. 2005: Ninteger v. 2.3 Fractional control toolbox for MatLab, 2005.

Venkataramanan, G. and **Divan, D.M.** 1990: Discrete time integral sliding mode control for discrete pulsemodulated converters. *21st Annual IEEE Power Electronics Specialists Conference*, 67–73, 11–14 June.

Vinagre, B.M., **Monje, C.A.** and **Calderon, A.J.** 2002: Fractional order systems and fractional order control actions. *41st IEEE International Conference on Decision and Control*, Las Vegas, NV, 10–13 December, pp. 15–38.

Xu, R. and **Özgüner, Ü.** 2008: Sliding mode control of a class of underactuated systems. *Automatica* 44, 233–41.

Young, K.D., **Utkin, V.** and **Özgüner, Ü.** 1999: A control engineer's guide to sliding mode control. *IEEE Transactions Control Systems Technology* 7(3): 328–42.